Lyotropic liquid crystal elastomers for drug delivery

Colloids and Surfaces B: Biointerfaces 226 (2023) 113304

Contents lists available at ScienceDirect

Colloids and Surfaces B: Biointerfaces

journal homepage: www.elsevier.com/locate/colsurfb

Lyotropic liquid crystal elastomers for drug delivery

Annija Stepulane [a,b], Kajsa Ahlgren [c], Adrian Rodriguez-Palomo [c,1], Anand Kumar Rajasekharan [b], Martin Andersson [a,b,*]

[a] Department of Chemistry and Chemical Engineering, Chalmers University of Technology, Gothenburg SE-412 96, Sweden
[b] Amferia AB, Astra Zeneca BioVentureHub c/o Astra Zeneca, Pepparedsleden 1, Mölndal SE-431 83, Sweden
[c] Department of Physics, Chalmers University of Technology, Gothenburg SE-412 96, Sweden

ARTICLE INFO

Keywords:
Polydimethylsiloxane
Elastomers
Lyotropic liquid crystals
Liquid crystal elastomers
Triblock copolymer
Polymer blending
Drug-delivery

ABSTRACT

Silicone elastomers like polydimethylsiloxane (PDMS) possess a combination of attractive material and biological properties motivating their widespread use in biomedical applications. Development of elastomers with capacity to deliver active therapeutic substances in the form of drugs is of particular interest to produce medical devices with added functionality. In this work, silicone-based lyotropic liquid crystal elastomers with drug-eluting functionality were developed using PDMS and triblock copolymer (diacrylated Pluronic F127, DA-F127). Various ternary PDMS–DA-F127–H_2O compositions were explored and evaluated. Three compositions were found to have specific properties of interest and were further investigated for their nanostructure, mechanical properties, water retention capacity, and morphology. The ability of the elastomers to encapsulate and release polar and nonpolar substances was demonstrated using vancomycin and ibuprofen as model drugs. It was shown that the materials could deliver both types of drugs with a sustained release profile for up to 6 and 5 days for vancomycin and ibuprofen, respectively. This works demonstrates a lyotropic liquid crystal, silicone-based elastomer with tailorable mechanical properties, water retention capacity and ability to host and release polar and nonpolar active substances.

1. Introduction

Silicone elastomers like polydimethylsiloxane (PDMS) possess a combination of properties that have made them indispensable tools in various industrial and biomedical applications. In their crosslinked state, silicone elastomers combine excellent material properties like flexibility, elasticity, chemical and thermal stability, optical transparency and gas permeability in combination with favourable biological properties like low toxicity [1]. Due to its biocompatibility in soft tissue applications, PDMS has been widely utilized for production of numerous types of medical devices like drains, shunts, urinary catheters, contact lenses and soft tissue implants [2,3]. However, when in contact with physiological fluids, PDMS materials suffer from nonspecific protein adsorption due to the high surface hydrophobicity. This makes PDMS susceptible to bacterial attachment, surface colonization and potentially infection [4]. In addition, because of the underlying chemical inertness, PDMS based materials are difficult to chemically functionalize to endow them with antibacterial or antifouling activity for infection prevention.

An essentially antagonistic biomaterial class to silicone are hydrogels – soft and hydrophilic 3D polymer networks capable of absorption and retention of large quantities of water, having attractive properties for a spectrum of biomedical applications. Water and nutrient transport, tunable biodegradability, viscoelasticity and mechanical properties similar to biological tissues have enabled the use of hydrogels in applications for encapsulation of therapeutic substances, as in-situ drug delivery vehicles, tissue engineering scaffolds, and as wound care products [5–8]. However, the lack of mechanical integrity limits the use of hydrogels in more structurally demanding applications like elastomeric materials. As a consequence, many studies have attempted to improve the mechanical properties of hydrogels not compromising on their functionality via careful control over the network architecture [9–12].

A relatively cost-effective alternative to new polymer material synthesis is polymer blending, where two or more, often dissimilar, polymers are blended to achieve new materials with improved properties. Blends can be broadly divided into three categories based on the

* Corresponding author at: Department of Chemistry and Chemical Engineering, Chalmers University of Technology, Gothenburg SE-412 96, Sweden.
E-mail address: martin.andersson@chalmers.se (M. Andersson).
[1] Present address: Interdisciplinary Nanoscience Center, iNANO, Aarhus University, Gustav Wieds Vej 14, 8000 Aarhus C, Denmark

https://doi.org/10.1016/j.colsurfb.2023.113304
Received 13 December 2022; Received in revised form 30 March 2023; Accepted 8 April 2023
Available online 10 April 2023

compatibility of the blended polymer phases – immiscible or heterogenous blends, compatible blends, and miscible or homogenous blends [13]. More often two polymers will tend to phase separate when mixed together due to their low miscibility between the separate components, resulting in distinct macro or microdomains of low interfacial adhesion, leading to compromised mechanical properties. To circumvent this, compatibility of polymer blends has been utilized to synthesize thermodynamically stable blends with the help of compatibilizing agents that increases the blend stability with the two phases. Commonly used compatibilizing agents are block or graft copolymers, which can reduce the interfacial tension between the two phases. Alternatively, polymer mixing can be controlled via the formulation of the blends and corresponding processing conditions; however, thermodynamic stability remains an issue with phase separation occurring over time [14].

Silicones are immiscible with most organic polymers, resulting in blends of poor stability. Instead stabilization is as an attractive strategy for synthesis of silicone containing blends with improved properties [15]. Many attempts have been made to blend silicone polymers with hydrophilic polymers in efforts to increase silicone's water affinity and permeability to active substances [16,17]. One alternative for the addition of hydrophilic moieties to silicone blends can be achieved by amphiphilic AB diblock or ABA triblock copolymer compatibilizers. Here the different blocks could be either of the same or different monomers as the silicone/hydrophile blend, relying on miscibility and physical entanglement for interphase stabilization [14,18]. By careful control over block copolymer concentration and molecular architecture, silicone blends with improved hydrophilicity, water retention and capacity for transport and release of hydrophilic substances can be produced [17].

Alternatively, some studies have investigated the potential of hydrogel reinforcement by phase separated hydrophobic domain incorporation into the hydrogel network, resulting in improvement of mechanical properties [12,19]. However, induced phase separation via blending as a strategy for improving physical properties remains common for silicone elastomer synthesis.

In recent years, there has been a growing interest in a class of materials known as liquid crystal elastomers (LCEs), which combine the elasticity of conventional elastomers such as silicone with the directional properties of liquid crystals (LCs). Liquid crystals are a mesophase, an intermediate state of matter between solid and liquid, that can spontaneously organize in a directional manner. There are two categories of LCs: thermotropic and lyotropic. Thermotropic LCs display mesophases in response to changes in temperature, while lyotropic LCs form mesophases as a result of changes in the concentration of a solvent [20,21]. The majority of LCEs are based on thermotropic LCs with limited attention devoted to lyotropic LCEs.

LCEs have demonstrated their versatility in a variety of biomedical applications [22,23] due to their unique mechanical, thermal, optical and responsive properties, with examples ranging from artificial muscles [24–26], tissue engineering scaffolds [20,27,28], actuators [29–33] and biosensors [34] to artificial irises [35], intervertebral discs [36], cardiovascular stents [37], implantable electronics [38] and as cell growth regulators [39,40].

In this work we have developed a synthetic polymer blend platform consisting of PDMS and amphiphilic ABA triblock copolymer in combination with water, to produced lyotropic liquid crystalline elastomeric materials of improved properties. We utilized diacrylated poly(ethylene oxide)−poly(propylene oxide)−poly(ethylene oxide) (DA−PEO_{100}−PPO_{70}−PEO_{100}−DA, DA-F127) copolymer known under the trade name Pluronic F127® as an amphiphilic compatibilizer.

Pluronic F127 is an amphiphilic triblock copolymer which contains ~ 70% PEO blocks contributing to its overall hydrophilic character. It is a biocompatible compound found in various pharmaceuticals, medical devices, cosmetics and food products. DA-F127 have been show to form solid hydrogels upon chemical crosslinking, capable of immobilization and release of different active substances – antimicrobial peptides, antibiotics, nonpolar drugs and DNA thanks to the amphiphilicity of the network structure [41–44].

Importantly, Pluronic F127 is well-known to self-assemble in the presence of polar and nonpolar solvents, where molecular segregation results in formation of distinct domains, forming a variety of lyotropic LC phases [45]. Further studies have investigated the potential of Pluronic – oil – water systems for their capacity to form self-assembled materials by incorporation of crosslinkable functional moieties, synthesizing tough elastomeric materials and bone nanocomposites with order structure [46,47]. Inspired by this work we aimed to develop a soft and elastic material by exploring the Pluronic F127 blending and self-assembly capabilities in presence of PDMS as the "oil" phase to produce functional materials capable of retaining the properties of the individual components.

The aim of the present study was to develop an elastomeric material by tailoring the mechanical properties and functionality of blends produced from PDMS and DA-F127 as LCEs capable of delivering active substances such as therapeutics. The compatibility and uniformity of DA-F127–PDMS–H_2O blends were explored by construction of a ternary phase diagram. Furthermore, three compositions were found to have unique properties of interest, as determined based on their optical transparency, macroscopic homogeneity, and mechanical strength. Their mechanical and structural properties were further characterized by tensile and compression testing, along with small angle X-ray scattering. The blend morphology was characterized with scanning electron microscopy, and the surface properties assessed by water contact angle analysis. The swelling capacity in water was evaluated, and the blends' capacity to deliver polar and nonpolar drugs was assessed using vancomycin and ibuprofen as model drugs. The findings of this study put forward a silicone-based lyotropic LCE with tailorable mechanical properties, water retention capacity and ability to host and release polar and nonpolar active substances.

2. Materials and Methods

Unless noted otherwise, all chemicals used in this study were purchased from Sigma Aldrich Sweden AB and used as received without further purification.

2.1. Preparation of DA-F127 – PDMS – H_2O blends

The materials were prepared by mixing DA-F127, PDMS prepolymer and water in different compositions inspired by the ternary phase diagram of Pluronic F127-water-"oil" systems reported elsewhere [45]. The DA-F127 copolymer powder (DA−PEO_{100}−PPO_{70}−PEO_{100}−DA, provided by Amferia AB) was mixed with Milli-Q water in different concentrations to form homogenous gels, adding 0.05 wt% photoinitiator Irgacure 2959 with respect to the copolymer weight. Resulting gels were refrigerated overnight at 4 °C to improve the DA-F127 solubility. Prior to the final mixing, gels were removed from the fridge and allowed to reach room temperature.

Separately, PDMS prepolymer was mixed using Sylgard 184 (Dow Corning) silicone elastomer kit in ratio 10 parts base agent to 1 part curing agent and degassed to remove any trapped air bubbles. Finally, DA-F127 gels were manually mixed with PDMS prepolymer according to the desired DA-F127–PDMS–H_2O concentration (e.g., to prepare DA-F127–PDMS–H_2O at a composition of 40–15–45 wt%, 0.85 g of 47.1 wt % DA-F127 hydrogel was first mixed, followed by addition of 0.15 g of the PDMS prepolymer to form 1 g of the final mixture). The resulting mixtures were cast between two glass slides using 1 mm thick spacers, followed by crosslinking via a two-step polymerization process. First samples were heat-cured at 37 °C for 24 h to facilitate the catalyst-induced hydrosilylation of PDMS, followed by free-radical photopolymerization of the DA-F127 at $\lambda = 365$ nm for 10 min. A visual evaluation of the as-prepared samples was conducted, and macroscopically homogeneous materials were chosen for further analysis based on

parameters like optical transparency and mechanical stability, with transparency indicating absence of phase separation and formation of single phase.

Pristine PDMS and DA-F127 hydrogels were prepared separately to be used as reference materials. For that, 30 wt% DA-F127 gels were mixed as previously described, refrigerated for 24 h and photo-polymerized at $\lambda = 365$ nm for 3 min forming solid hydrogels. The PDMS was prepared using the Sylgard 184 silicone elastomer kit as previously described, degassed, cast in a glass petri dish and heat cured for 24 h at 37 °C to form solid elastomer.

2.2. Material characterization

2.2.1. Tensile and compression testing

The materials chosen for analysis were first evaluated under tensile and compressive deformation using an Instron 5600 UTM universal testing machine.

For tensile testing, 1 mm thick sample sheets were prepared as previously described with the addition that prior to the casting between the glass slides gels were centrifuged at 5000 rpm for 10 min to remove any trapped air bubbles. Dog bone shapes with dimensions of 8 mm gauge width and 20 mm gauge length were punched out from the as-prepared polymerized sheets. The samples were stretched at constant strain rate of 10 mm/min until fracture, using a 100 N load cell and the resulting stress-strain curves were recorded. Young's modulus was calculated from the linear region of the recorded curves. As controls, pure PDMS elastomers polymerized at 37 °C for 24 h, as well as 30 wt% DA-F127 hydrogels were included in the measurements. This was to account for each polymer's contribution to the tensile strength of the blend.

For compression testing, gels were cast into glass vials 13 mm in diameter prior to polymerization and centrifuged at 5000 rpm for 10 min to remove any air bubbles. The gels were polymerized as previously described forming cylindrical shapes that were harvested by carefully breaking the vials, and the samples cut to height of 5 mm. Samples were uniaxially compressed to 80% deformation at a strain rate of 10 mm/min, or until the limit of the load cell (5 kN) was exceeded. The resulting stress-strain curves were recorded, and the compressive modulus was calculated from the linear region of the recorded curves. Similarly, pure PDMS sample polymerized at 37 °C, as well as DA-F127 hydrogel were measured to account for each polymer's contribution to the compressive strength. All measurements were performed in triplicates.

To evaluate the impact of water uptake and swelling on the mechanical properties of the test compositions, the as-prepared samples were preswollen in Milli-Q water for varying durations (2, 4, 6, 24, 48, 72, and 120 h) before being subjected to compression testing. Similarly, samples were uniaxial compressed at a strain rate of 10 mm/min until 80% compression was achieved or until fracture occurred. The compressive strength and modulus were determined by analysing the recorded stress-strain curves and compared across different swelling time points. All measurements were performed in duplicates.

2.2.2. Water contact angle analysis (WCA)

Water contact angle and surface wetting properties of the as-prepared materials were analysed with optical tensiometer (Theta, Attention) operated in static contact angle mode. A droplet of Milli-Q water was manually dispensed onto the materials' surface and high-resolution camera used to record droplet spreading over 5 min. Contact angle changes were determined from the recorded images using OneAttension software. All measurements were performed in triplicates.

2.2.3. Scanning electron microscopy (SEM)

Sample microstructure was investigated using scanning electron microscopy (Leo Ultra 55, Carl Zeiss AG). SEM was operated at 2 kV accelerating voltage and a secondary electron detector was used for imaging. The as-prepared samples were cut with a microtome blade to obtain cross-sectional images and sputter coated with gold for 1 min at 10 mA prior imaging.

2.2.4. Small-angle X-ray scattering (SAXS)

The structural characterization was performed using SAXS on unpolymerized gel mixtures as well as the as-prepared polymerized sheets. A Mat:Nordic instrument (SAXSLAB) with a Rigaku MicroMax-003+ Cu-radiation MicroMax-003 + Cu-radiation source was employed at the Chalmers Micro-Analysis Laboratory (CMAL, Sweden) over a q range of 0.00138 – 0.30659 $Å^{-1}$, with an X-ray wavelength of $\lambda = 1.54$ Å. The measurements were conducted in vacuum with an exposure time of 15 min per sample.

Synchrotron radiation SAXS was carried out at the cSAXS beamline, Swiss Light Source, at the Paul Scherrer Institute (PSI, Switzerland). A monochromatic beam of 11.2 eV (1.107 Å) was defined using a fixed-exit double crystal Si (111) and focused vertically by a bendable Rh-coated mirror and horizontally by bending the second monochromator crystal. An in-vacuum flight tube with a length of 2 m was placed between the sample and the detector to minimize the air scattering and absorption. The scattering signal was recorded by a Pilatus 2 M detector (1475 ×1679 pixels, 172 ×172 μm^2 per pixel) after the flight tube [48, 49].

The recorded scattering peaks were fitted to a Gaussian fit to acquire the peak position at maximum and the average micellar dimension d calculated using Eq. 1:

$$d = \frac{2\pi}{q} \tag{1}$$

where q signifies the q-position of the recorded peaks.

2.2.5. Swelling measurements

The as-prepared samples swelling capacity in Milli-Q water was studied over time. Samples were immersed in Milli-Q water to facilitate the swelling of the DA-F127 portion of the polymer matrix, followed by weight measurements every hour for the first 6 h, then once a day for 7 days. The swollen weight W_t as well as the initial dry weight W_0 were recorded, and the swelling ratio depending on time $S_{w,t}$ calculated using Eq. 2:

$$S_{w,t} = \left(\frac{W_t - W_0}{W_0}\right)100 \tag{2}$$

2.3. Drug delivery

The chosen compositions were studied for their capacity to deliver polar and nonpolar drugs from the materials, with vancomycin chosen as the polar, and ibuprofen as the nonpolar model drug. Prior the drug loading, circular samples 4 mm in diameter were punched out from the polymerized sheets with a biopsy punch and washed in chloroform for 48 h to remove any unpolymerized fractions. The samples were then vacuum dried at room temperature, and the dry weight recorded. The dried samples were subsequently loaded with vancomycin or ibuprofen, separately.

For loading ibuprofen, samples were placed in separate vials containing 1 ml of 10 wt% ibuprofen solution in acetone and equilibrated for 72 h, following an intermediate rinsing step in pure acetone and air drying at 37 °C for 1 h. For elution, ibuprofen samples were immersed in 3 ml of 1 wt% SDS solution in Milli-Q water to facilitate the ibuprofen solubility and placed on a platform shaker. The absorption signal from elution media was measured using a UV-Vis spectrophotometer (Multiskan™ GO, Thermo Fisher Scientific) at $\lambda = 272$ nm every 15 min for the first 4 h, then twice a day for 3 days and once a day until no further elution could be recorded. The actual amount of ibuprofen eluted was calculated from a previously constructed standard curve. To account for sample degradation interfering with the absorption signal, each experiment included a drug-free sample as reference.

For loading vancomycin, the washed and dried samples were placed

in separate vials containing 1 ml of 1 wt% vancomycin solution in Milli-Q water for 72 h. Afterwards samples were rinsed in pure Milli-Q water for 1 – 2 min to remove any loosely adsorbed drug and air dried at 37 °C for 24 h recording the final dry weight. For elution, vancomycin-loaded samples were placed in vials containing 6 ml pure Milli-Q water and placed on a shaker plate. Elution media was sampled, and absorption measured at $\lambda = 280$ nm every 15 min the first 4 h then twice a day until no further elution could be detected. A drug-free sample was included in each experiment to account for the polymer degradation.

Both drug delivery measurements were repeated three times in a triplicate per sample composition type (n = 9).

2.4. 3D printing

Extrusion 3D printing was utilized to assess the chosen composition's viscoelastic properties along with capabilities to be processed in macroscopical objects of high resolution at ambient conditions. For this, unpolymerized gels were loaded in UV protected syringe and centrifuged at 6000 rpm for 10 min to remove any trapped air bubbles. The syringes were loaded in the printing cartridge and gels printed with pneumatic extrusion-based 3D bioprinter (INKREDIBLE™, Cellink) at room temperature. A hollow cylinder and a human nose model were printed. The resulting objects were crosslinked by first exposing it to UV light ($\lambda = 365$ nm) for photopolymerization of the DA-F127 fraction, followed by heat curing for 24 h at 37 °C for the PDMS fraction.

3. Results and Discussion

3.1. Material preparation and phase diagram construction

In this study different compositions of the ternary DA-F127–PDMS–H_2O system were investigated covering a wide area of the Pluronic–oil–water ternary phase diagram. Here the Pluronic F127 self-assembly is used as an inspiration for synthesis of new types of polymer blends in combination with PDMS prepolymer as the nonpolar, and water as the polar "solvents".

To screen for promising compositions, qualitative assessment was performed of the as-prepared materials based on visual properties like optical transparency, macroscopic homogeneity (visual phase separation) and mechanical stability. Based on this, an optically transparent composition region could be detected in the central part of the phase diagram as seen in Fig. 1**A** with the prepared compositions forming relatively robust materials. The opaque samples exhibited macroscopic phase separation post crosslinking, were mechanically fragile or did not form solid materials, therefore they were discarded for further analysis. The effect of the composition on the material's turbidity can be seen, with an increase in DA-F127 and PDMS concentration resulting in increased transparency as seen between samples 1 – 5 (Fig. 1**B**).

From the evaluation of the phase diagram, three compositions of interest were found (composition B, D and H) and chosen for further analysis. The materials were mechanically stable with low opacity (see Fig. 1**C**). The transparency was generally utilized as an indicator of a homogenous phase. Sample B and D composed of DA-F127–PDMS–H_2O

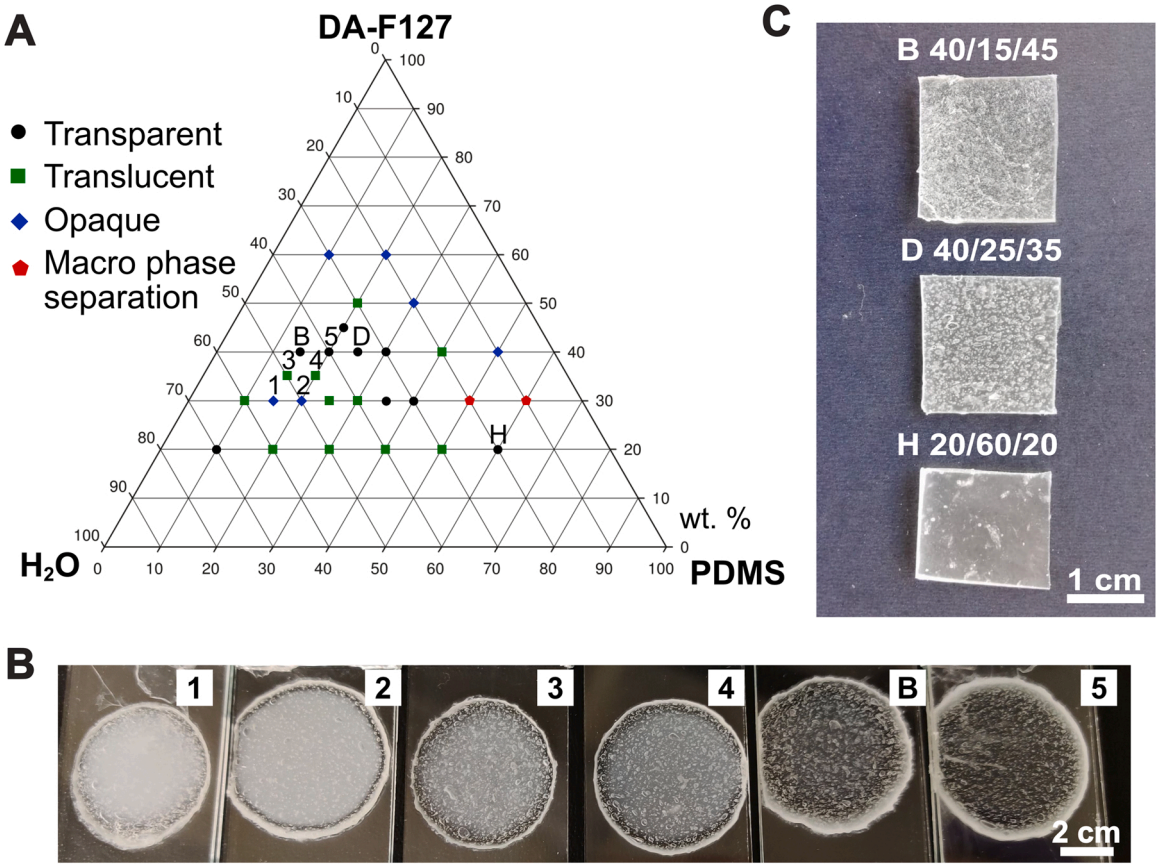

Fig. 1. (A) Ternary phase diagram of DA-F127–PDMS–H_2O materials constructed based on the prepared compositions and their visual evaluation after polymerization. Black dots indicate materials that were homogeneous and transparent, green squares indicate compositions that exhibited intermediate transparency, blue diamonds indicate fully opaque samples, red polygons indicate compositions exhibiting macroscopic phase separation. (B) Example of the composition concentration effect on the material transparency on samples polymerized between glass slides including composition B (40–15–45 wt%) chosen for further analysis. (C) Photograph of the as-prepared compositions B (40–15–45 wt%), D (40–25–35 wt%) and H (20–60–20 wt%) chosen for further analysis. Air bubbles were present in composition B and D.

at a concentration of 40–15–45 wt% and 40–25–35 wt%, respectively, were chosen to assess the effect of relatively low PDMS concentration. Furthermore, sample H with a composition of 20–60–20 wt% was chosen due to the PDMS rich region being of particular interest for functional elastomeric material development, having mechanical properties similar to pure PDMS.

3.2. Structural analysis

The selected compositions B (40–15–45 wt%), D (40–25–35 wt%) and H (20–60–20 wt%) in their unpolymerized gel state, were examined using SAXS. The integrated scattering intensity of each sample prior polymerization showed an intense peak at $q = 0.043 - 0.044$ Å^{-1} seen in Fig. 2**A**, suggesting the presence of a micellar arrangement with an average micellar dimension of 143 – 147 Å (peak positions in Supplementary information, Table S1). The unpolymerized gel mixtures with compositions B and D displayed additional peaks at $q \approx 0.060$ Å^{-1} and $q \approx 0.074$ Å^{-1}. Those peaks were identified as the diffraction peaks of a self-assembled phase. The peak position followed a ratio of $1:\sqrt{4/3}:\sqrt{8/3}$, suggesting a cubic self-assembled phase. However, those diffraction peaks were absent in the sample H, where spherical micelles with no specific long-range arrangement can be expected. Additionally, the reference unpolymerized 30 wt% DA-F127 gel showed four characteristic peaks at $q \approx 0.043$ Å^{-1}, $q \approx 0.060$ Å^{-1} $q \approx 0.067$ Å^{-1} and $q \approx 0.074$ Å^{-1}. While there is a possibility of detecting further peaks at lower q values, their clear resolution from the background noise presented a challenge. Nonetheless, the observations made provide substantial evidence for the presence of a micellar cubic phase in DA-F127 hydrogel, consistent with analogous Pluronic F127 – alkanol – water systems as reported by P. Holmqvist et al. [50,51].

Lyotropic LC systems based on surfactants can present challenges in the process of peak indexation and determination of crystallographic space group. This is due to the low peak intensity, which is often inherent in liquid crystalline materials. As previously reported by P. Holmqvist et al., the peak positions and their relative intensities can provide valuable information regarding the space group of the system. In particular, the first peak observed at $q \approx 0.043$ Å^{-1} is typically the most intense in primitive cubic space group and can be attributed to *hkl* = 111 reflections, which is consistent with our observations. Additionally, the peaks at $q \approx 0.060$ Å^{-1} and $q \approx 0.074$ Å^{-1} could be indexed as (211) and (220) reflections, respectively [50]. However, it is important to note that the presence of the $q \approx 0.067$ Å^{-1} peak was not observed in this previously reported study.

In a similar surfactant system reported by B. Svensson et al. authors have suggested the primitive Pm3n space group [52]. They showed four peaks at q ≈ 0.043 Å^{-1}, q ≈ 0.060 Å^{-1}, q ≈ 0.067 Å^{-1} and q ≈ 0.074 Å^{-1} indexed as (200), (220), (310) and (222) reflections, respectively, coinciding with our data for the DA-F127 sample. However, they also observed additional peaks: (110), (210) and (211), which were absent in our diffraction patterns.

Overall, our results suggest that the peaks observed in 30 wt% DA-F127 hydrogel, sample D and possibly sample B, can be ascribed to a primitive cubic structure. However, the absence of additional peaks in samples H and the low resolution of additional peaks in sample B could be attributed to noise and random X-ray scattering resulting from the high PDMS content. Additionally, the distortion of the spherical micellar geometry, as reported in several studies, is a possible contributing factor [52,53].

Subsequently, an equivalent set of samples were measured after the two-step polymerization process. The scattering intensity shown in Fig. 2**B** presented a main scattering peak as previously seen in Fig. 2**A**; however, there was no presence of additional peaks. The lack of additional diffraction peaks in samples B, D and DA-F127 may indicate random scattering due to crosslinking or, to a lesser extent, loss of order in the system after polymerization. The peak position for the three samples had minor variations, possibly due to slight changes in the water content during the measurement, which may produce swelling/shrinking of the micellar structure. Increasing peak broadening was also observed as a sign of a broader micellar size distribution in the material, possibly caused by the increasing concentration of PDMS in the material. It can therefore be concluded that the micellar structure was kept after polymerization, however no indications as to the long-range order in the material structure can be made.

Additionally, the reference 30 wt% DA-F127 crosslinked hydrogel displayed a single scattering peak coinciding with samples B, D and H, with similar loss of the secondary diffraction peaks seen in the unpolymerized 30 wt% DA-F127 gel. Similar observations have been reported previously with 35 wt% DA-F127 hydrogels, where micellar cubic structure present in the gel form has been retained after crosslinking, however resulting in loss of scattering intensity and secondary peak signal due to crosslinking [47].

3.3. Scanning electron microscopy

The as-prepared sample cross-sections were imaged with SEM to investigate the compositional effect on the resulting microstructure (see

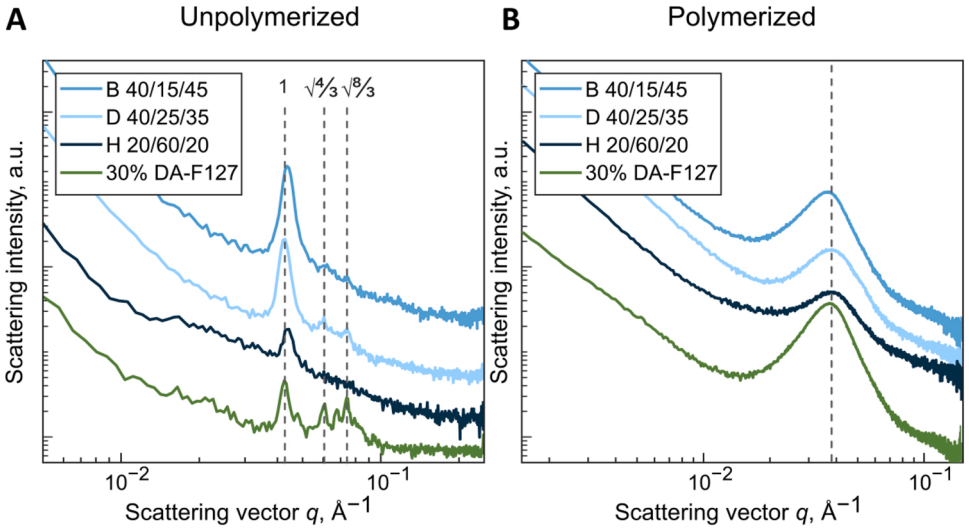

Fig. 2. (A) Integrated intensity of the SAXS pattern of the compositions B (40–15–45 wt%), D (40–25–35 wt%) and H (20–60–20 wt%) prior polymerization and (B) post polymerization. 30 wt% DA-F127 unpolymerized gel and crosslinked hydrogel included as a reference. Patterns have been shifted vertically for clarity.

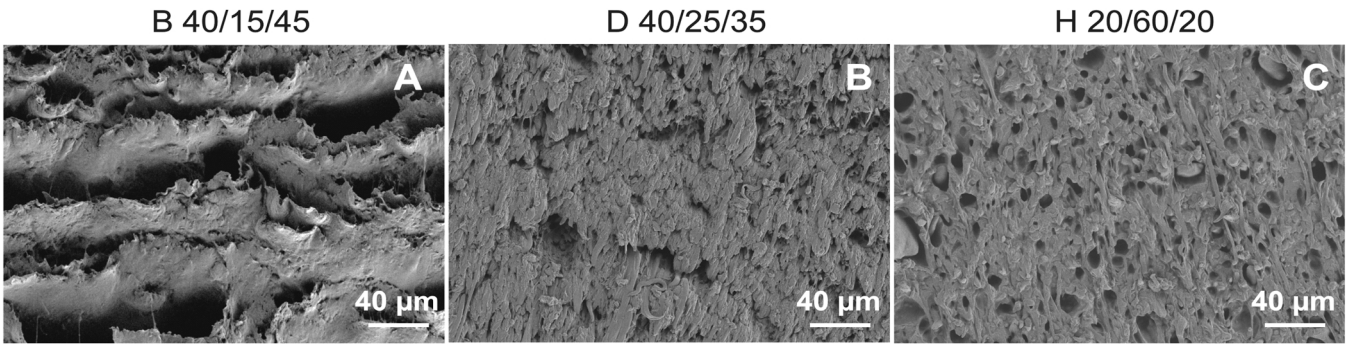

Fig. 3. SEM micrographs of the as-prepared composition cross-sections for samples B (40–15–45 wt%), D (40–25–35 wt%) and H (20–60–20 wt%).

Fig. 3). The micrographs demonstrate a notable effect that the compositional variation has on the structural homogeneity, density, and porosity of the test samples.

Sample B displayed a heterogenous flaky morphology having interlocked irregular pores of micrometre size. Considering the high DA-F127 and water content, low network density and high porosity can be expected, resembling a microstructure of LCs. Sample D demonstrated higher density as a consequence of increased PDMS content. Additionally, thread-like features around 2 – 4 μm in size can be seen intertwining throughout the cross section, potentially indicating different phases. Generally, the morphology resembles that of miscible polymer blends with continuous distribution of one phase (PDMS) inside the other (DA-F127), with additional porosity potentially remnant of water phase. Ultimately sample H displayed morphological characteristics of typical immiscible blends, where microphase segregation can be seen. Although highly crosslinked, the material contains discrete regions of low interfacial bonding, potentially indicating the phase separation between PDMS as the continuous phase and DA-F127–water as the dispersed phase. It should, however, be emphasized that SEM is performed under vacuum conditions on dried samples, which could alter the microstructural features observed.

3.4. Mechanical testing

The as-prepared compositions were investigated under tensile and compressive deformation and their mechanical properties compared to pristine PDMS and a reference 30 wt% DA-F127 hydrogel (Fig. 4).

It can be seen from the recorded tensile deformation stress-strain curves (Fig. 4**A**) that samples B and D exhibit similar mechanics to the reference DA-F127 hydrogel, with moderate strength, stiffness and

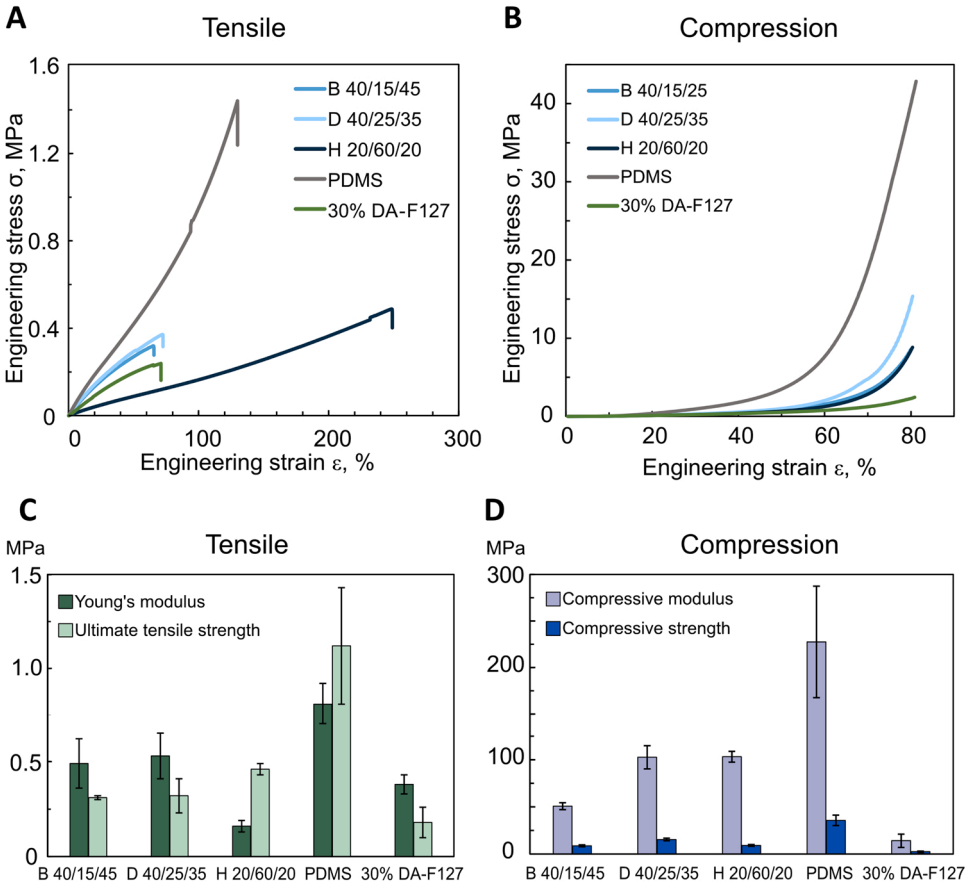

Fig. 4. (A) Tensile and (B) compression deformation stress-strain curves of the different compositions. Calculated (C) tensile and (D) compressive parameters of the as-prepared samples. Compressive modulus calculated from the steepest section of the stress-strain curves.

elasticity compared to pristine PDMS. The Young's modulus (see Fig. 4**C**) has increased for samples B and D ($E_B = 0.49 \pm 0.13$ MPa and $E_D = 0.53 \pm 0.12$ MPa) compared to pure DA-F127 hydrogel ($E_{DA\text{-}F127} = 0.38 \pm 0.05$ MPa) as a consequence of the PDMS fraction and water content reduction. Additionally, a moderate increase in the ultimate tensile strength can be observed ($\sigma_{DA\text{-}F127} = 0.18 \pm 0.08$ MPa → $\sigma_B = 0.31 \pm 0.01$ MPa and $\sigma_D = 0.32 \pm 0.09$ MPa). A drastically different tensile behaviour can be seen for sample H, where low stiffness and moderate strength is accompanied by a significant increase in elasticity ($\varepsilon_H \sim 240\%$) – 2 times greater than PDMS ($\varepsilon_{PDMS} \sim 112\%$) and 3.5 times greater than DA-F127 ($\varepsilon_{DA\text{-}F127} \sim 68\%$). Such drastic increase in elasticity could potentially be associated with lower degree of crosslinking and increased polymer chain length in the PDMS fraction. Moreover, microstructure features like porosity have been previously shown to affect the mechanical properties of porous elastomers, with higher porosity also exhibiting higher deformability [54]. Considering the porous structure of sample H observed with SEM, potential effects on the elasticity could be explained.

Furthermore, the samples were analysed under compression, and the compressive strength at maximum as well as the compressive modulus at high strain ($\varepsilon \geq 70\%$) were determined from the recorded stress-strain curves to compare the differences in compressive behaviour (Fig. 4**B**). Low stiffness at low strain can be observed for all three test compositions B, D and H, including the DA-F127 hydrogel, with pristine PDMS being notably stiffer. By increasing the strain, a deviation in the stress response between the material types can be seen. Sample B displayed a moderate increase in compressive strength accompanied by a significantly increased compressive modulus ($\sigma_B = 8.58 \pm 0.93$ MPa and $E_B = 50.63 \pm 3.67$ MPa) compared to DA-F127 hydrogel (Fig. 4**D**). Sample H displayed a relatively similar compressive strength ($\sigma_H = 9.00 \pm 0.95$ MPa), however displayed a sharper increase in the compressive modulus ($E_H = 103.23 \pm 5.70$ MPa). Notably, sample D exhibited the most significant enhancement in the mechanical properties with increased compressive strength and modulus ($\sigma_D = 15.28 \pm 1.47$ MPa and $E_D = 102.59 \pm 12.37$). Comparatively, the reference PDMS exhibits high strength and stiffness ($\sigma_{PDMS} = 35.65 \pm 5.53$ MPa and $E_{PDMS} = 227.52 \pm 59.95$ MPa), consistent with earlier reported values. The compressive characteristics of the DA-F127 hydrogel were found to be the poorest ($\sigma_{DA\text{-}F127} = 2.41 \pm 0.70$ MPa and $E_{DA\text{-}F127} = 13.08 \pm 7.16$ MPa), likely due to high water content and brittle nature.

The compressive and tensile characteristics of the different compositions relates to the characteristics of the individual components. With PDMS being very flexible and elastic polymer, whilst DA-F127 hydrogel being soft and brittle, an intermediate behaviour can be seen in the prepared samples, where samples D and H exhibits more rubber-like behaviour compared to samples B, that display the weakest mechanics due to the high DA-F127 and water content. Furthermore, it is possible that the mechanical response of the compositions could be influenced by the nano and microstructural features of the material. However, more comprehensive investigations are necessary to accurately determine the magnitude of this effect.

Ultimately it can be seen that by varying of the DA-F127–PDMS–H_2O ratio in the as-prepared compositions, mechanics could be tailored, offering potential for improving the mechanical properties compared to the individual components.

3.4.1. Swelling impact on the compressive properties

To evaluate the impact of water absorption and material swelling on the mechanical characteristics of the test compositions, the as-prepared samples were immersed in Milli-Q water for different durations. Afterwards, compression testing was performed, and the results were compared to those obtained from the reference 30 wt% DA-F127 hydrogel. The calculated values of compressive strength and moduli are depicted in Fig. 5 with the recorded stress-strain curves and tabulated compressive parameters found in Supplementary information Fig. S1 and Table S2, respectively.

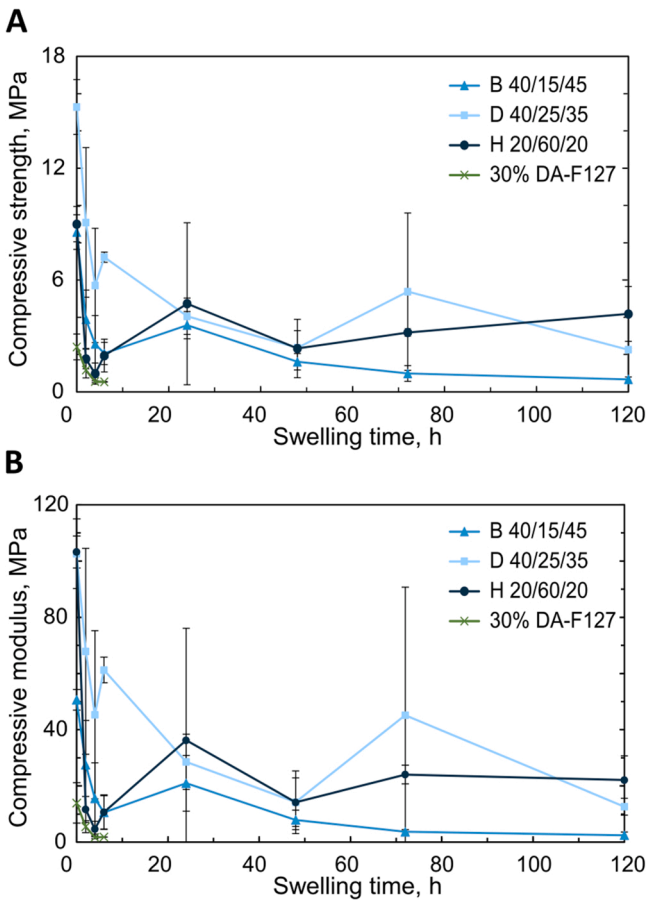

Fig. 5. Compressive properties of the test compositions B (40–15–45 wt%), D (40–25–35 wt%), H (20–60–20 wt%) and the reference 30 wt% DA-F127 hydrogel determined as a function of swelling time in water. (A) Compressive strength and (B) compressive modulus calculated from the recorded stress-strain compression curves.

It can be seen from the recorded stress-strain curves (Fig. S1) that majority of the test specimens retained their mechanical integrity after a swelling period of 120 h. Exceptions were observed for sample B and DA-F127 hydrogel displaying brittle fraction after 48 and 4 h of swelling, respectively.

The water uptake in the initial 6 – 24 h was observed to have a significant impact on the compressive parameters of all test samples (see Fig. 5). A rapid reduction in both mechanical strength and stiffness for all test compositions was observed, most likely due to the rapid increase in water uptake during this period. This correlation was found to be consistent with water swelling measurements, as further outlined in Section 3.6. The reference DA-F127 hydrogel exhibited a similarly rapid reduction in mechanical strength, suggesting that the swelling of the DA-F127 network is a key governing factor in the observed changes in compressive behaviour for all test compositions. Notably, the mechanics of sample B were observed to decrease to a level comparable to that of the DA-F127 hydrogel after 48 – 72 h. Additionally, sample B was found to be the mechanically weakest among the test samples, which may be attributed to highest content of DA-F127 and water, and lowest PDMS fraction.

The mechanical properties of samples D and H were found to remain relatively high even after 120 h of swelling in water. This observation is consistent with the mechanical properties of the as-prepared samples, however unexpected given the high water swelling degree of sample D, as discussed in Section 3.6. Overall, sample D displays the most robust mechanics over the swelling period. Although, it should be noted that significant variations were observed in the measurements, potentially

due to macroscopic defects in the compression samples resulting from the preparation of the highly viscous gels prior crosslinking. Similarly, sample H was found to be mechanically stable, as expected due to high PDMS content.

In summary, these findings underscore the significance of regulating the hydrophilic and hydrophobic composition fractions, as well as the DA-F127–PDMS–H_2O ratio, in the test compositions, and their influence on the uniformity of mechanical properties under wet conditions. These properties are especially relevant for potential biomedical applications that involve contact with aqueous environments.

3.5. Water contact angle

The surface wetting properties of the as-prepared compositions were determined with WCA analysis over a 5 min period and compared to pristine PDMS and 30 wt% DA-F127 hydrogel as controls (Fig. 6). Pristine PDMS cured at 37 °C displayed stable hydrophobic character over the measurement period with the average WCA of 105.7 ± 1.8°. The reference DA-F127 hydrogel displayed an expected change from the initial WCA of 101.2 ± 2.0° to 82.4 ± 6.0°, consistent with the amphiphilic character of Pluronic F127 backbone. All three test compositions demonstrated higher initial hydrophobicity than the controls, with WCA of 115.9 ± 2.4°, 115.8 ± 3.7°, 119.1 ± 3.4° for sample B, D and H, respectively. Samples B and D displayed a slower wetting rate compared to sample H with WCA reaching that of pristine PDMS after ~ 5 min (sample B – 108.8 ± 13.3°, sample D – 105.9 ± 1.4°). With compositions B and D containing relatively more DA-F127 (40 wt%) the wetting pattern consequentially resembles that of reference DA-F127 hydrogel, with slower water uptake in the material structure. Sample H demonstrated a more rapid initial reduction in WCA, followed by stable WCA over 5 min of 99.7 ± 5.3°. Whilst being the most PDMS-rich, sample H displays WCA values lower than pristine PDMS, suggesting DA-F127 presence on the material surface. Although being more PDMS lean, samples B and D displayed overall higher surface hydrophobicity, indicating inversed surface chemical characteristics when compared to the bulk of the material. Additionally, the microstructural differences observed with SEM could result in changes in increased surface roughness – a potentially contributing factor to the increased hydrophobicity of samples B and D.

3.6. Swelling in water

The swelling behaviour in Milli-Q water of the samples B, D and H was analysed and compared to the reference DA-F127 hydrogel (Fig. 7**A**). As evident from the swelling curves, stable hydration profile

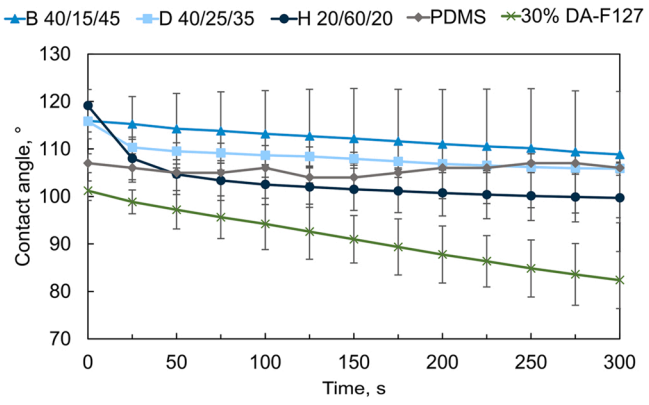

Fig. 6. Water contact angle analysis of the as-prepared samples, pristine PDMS and 30 wt% DA-F127 hydrogel. Samples B (40–15–45 wt%) and D (40–25–35 wt%) display increased surface hydrophobicity compared to pristine PDMS.. Sample H (20–60–20 wt%) display reduced hydrophobicity compared to pristine PDMS.

for all test compositions could be observed up to 7 days, indicative of sample stability in water medium. All samples retained their weight with no notable mass loss, confirming dense crosslinking between the phases. Additionally, all test samples displayed varying degree of water uptake over time, dependent on the material composition. The three test compositions displayed a more gradual water uptake compared to the 30 wt% DA-F127 hydrogel, by reaching the equilibrium water content around 72 h, contrary to rapid hydration of the DA-F127 hydrogel reaching equilibrium in around 4 h. With samples B, D and H containing 45, 35 and 20 wt% water, respectively, slower water uptake points toward the higher degree of crosslinking in these systems. Contrary to the WCA measurements, samples B and D show significantly higher degree of swelling compared to sample H, with equilibrium swelling degree around 270%, 170% and 55% for sample B, D and H, respectively. By tailoring the material composition and consequently the DA-F127–PDMS–H_2O ratio, materials with variable swelling degree can be obtained. As evident from samples B and D at a constant DA-F127 concentration, 10 wt% reduction in PDMS content can result in 100% increase in swelling degree.

3.7. Controlled drug delivery

The capacity of the chosen compositions B, D and H to act as carriers of polar and nonpolar drugs was investigated by monitoring drug release behaviour over time. Vancomycin and ibuprofen were chosen as the model polar and nonpolar drugs, respectively, with vancomycin being a highly water soluble (50 mg/ml) glycopeptide antibiotic and ibuprofen being nonsteroidal anti-inflammatory drug of low water solubility (0.011 mg/ml) [55]. Due to the amphiphilic nature of the DA-F127–PDMS–H_2O system it was hypothesized that drugs of different chemical polarity could be selectively loaded in the hydrophilic and hydrophobic domains of the materials' structure, resulting in retained release behaviour over time. Here it was suggested that the DA-F127 micelles in the material structure could serve as depots for vancomycin loading in the hydrophilic exterior of the micelles, while the micelle hydrophobic interior, along with the hydrophobic domains of PDMS could serve as ibuprofen reservoirs. The vancomycin and ibuprofen release curves from samples B, D and H can be seen in Fig. 7**B** and **C**.

For vancomycin release samples B and D demonstrate ~ 250% increase in delivered dose compared to sample H, most likely stemming from the high DA-F127 and water content in these materials (Fig. 7**B**). Sample D demonstrated a sustained release profile for around 6 days, similar to sample B nearing equilibrium saturation after 7 days. The backbone of the DA-F127 structure is dominated by the hydrophilic PEO blocks over the hydrophobic PPO blocks, rendering it more hydrophilic in character. This characteristic, along with the self-assembly behaviour and the thermoreversible gelling properties have been previously widely utilized to deliver hydrophilic substances like vancomycin from Pluronic F127 gels [56]. Considering the micellar arrangement in the sample B and D structure as determined by SAXS, vancomycin is most likely retained in the hydrophilic DA-F127 micellar domains throughout the continuous material structure. The sustained release trend over 6 days could be explained by the additional PDMS fractions enforcing the network structure and increasing the crosslinking density.

Contrary to samples B and D, sample H shows a minor burst release in the first few hours, reaching plateau with no additional drug delivered afterwards. This could potentially indicate loosely bound drug present on the material surface and in the material pores in immediate vicinity to the surface, with no significant distribution in the bulk. Considering the high PDMS content of sample H, along with water being used as the loading medium for the vancomycin, most of the drug is not capable of penetrating the material bulk and remains located close to the surface.

Similar release pattern can be observed for ibuprofen, with samples B and D delivering significantly higher drug dose compared to sample H (Fig. 7**C**). Samples B and D display an initial burst release after 4 h followed by a gradual release with equilibrium reached after ~ 5 days,

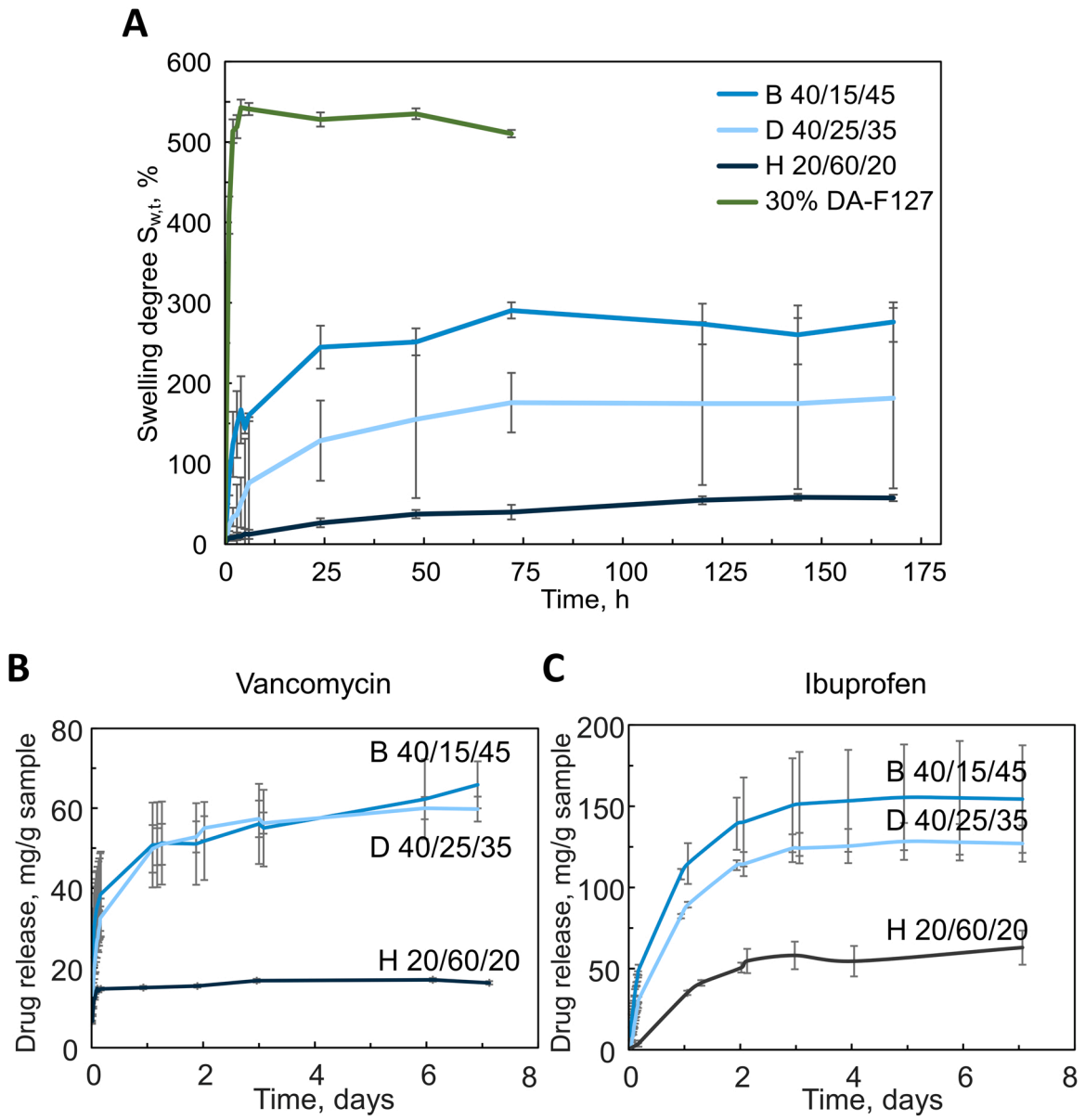

Fig. 7. (A) Degree of swelling in water for the as-prepared samples B (40–15–45 wt%), D (40–25–35 wt%), H (20–60–20 wt%) and the reference 30 wt% DA-F127 hydrogel. (B) Drug release pattern of vancomycin in Milli-Q water, and (C) ibuprofen in 1 wt% SDS buffer from the samples B (40–15–45 wt%) and D (40–25–35 wt %) and H (20–60–20 wt%).

whilst sample H reaches maximum delivery at around 3 days.

Similar to vancomycin release curves, the ibuprofen loading into samples B and D seem to be governed by the high DA-F127 and water content. By combination of the hydrophobic domains of the micellar interior with the hydrophobicity of the ibuprofen molecules, the more sustained drug release pattern can be explained. Similar to the water swelling measurements, it is clear that increase in the PDMS fraction by 10 wt%, results in reduction of the drug loading capacity with the amount of ibuprofen loaded reduced by ~ 17%.

Overall, it is clear that by using acetone as the loading medium, significantly higher encapsulated ibuprofen dose can be achieved in all compositions due to the increased ibuprofen solubility combined with the increased polymer network swelling. Although acetone is a good solvent for swelling PDMS, it is not sufficient to achieve high drug loading in the PDMS rich sample H alone, compared to the DA-F127 rich samples B and D. A potential explanation is the high concentration of micelles as a contributing factor to the hydrophobic drug retention than simple loading in the bulk of the hydrophobic PDMS network.

3.8. Material processing via 3D printing

Ultimately, as a proof-of-concept experiment, composition B was chosen to demonstrate its 3D printing capabilities in order to produce macroscopical objects with high resolution. As can be seen in Fig. 8 it was possible to 3D print a capillary tube and scaled-down human nose model using extrusion 3D printing, resulting in high level of precision. This result demonstrates how DA-F127 addition in the blend composition facilitates the viscoelastic properties needed for processing via 3D printing. Lyotropic LC gels are known to possess the rheological properties relevant in 3D printing by being inherently viscous, however able to flow during shearing of the extrusion process and recover upon removal of the shear force [46,57]. It is therefore expected that the blend compositions with high DA-F127 content like the composition B would display the necessary viscoelasticity in the unpolymerized gel state aiding the 3D printing process. Although further investigations are required, this result can serve as an early proof, showing how the developed material platform could function as a 3D printable elastomer

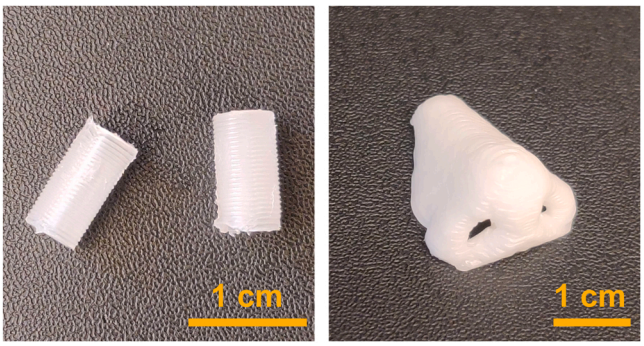

Fig. 8. Crosslinked 3D printed constructs of a capillary tube and scaled-down human nose from sample B (40–15–45 wt%). Samples turn opaque after drying.

with customised geometries for different applications.

4. Conclusions

In summary, this study presents the development of a material platform for production of lyotropic liquid crystal elastomers with tailorable mechanics and capacity to deliver both polar and nonpolar active substances, based on PDMS, DA-F127 and water. Different ternary PDMS–DA-F127–H_2O blend compositions were explored based on the material homogeneity and stability. Three compositions of interest were structurally characterized using small-angle X-ray scattering, revealing the presence of DA-F127 micelles in the blend system of varying size distribution. Furthermore, scanning electron microscopy imaging displayed significant morphological variation amongst the test compositions. Additional mechanical characterization via tensile and compression testing demonstrated tailorable mechanics dependent on the blend concentration and swelling time in water. The introduction of the DA-F127 in the elastomeric blend system resulted in increased water uptake and swelling capacity as demonstrated in water swelling measurements. Ultimately, the capacity for encapsulation and release of polar and nonpolar drugs from the test compositions was demonstrated using vancomycin and ibuprofen as model drugs. The findings of this study present a new type of silicone-hydrogel blend platform with tailorable mechanical properties, water retention capacity and ability to deliver different types of drugs independent of polarity.

CRediT authorship contribution statement

AS: Methodology, Investigation, Visualization, Data curation, Supervision, Writing – original draft. **KA:** Methodology, Investigation, Data curation. **ARP:** Methodology, Investigation, Writing – original draft. **AKR:** Supervision, Writing – review & editing. **MA:** Conceptualization, Writing – review & editing, Funding acquisition.

Declaration of Competing Interest

The authors declare the following financial interests/personal relationships which may be considered as potential competing interests, Annija Stepulane reports financial support and equipment, drugs, or supplies were provided by Amferia AB. Anand Kumar Rajasekharan reports financial support was provided by Amferia AB. Martin Andersson reports a relationship with Amferia AB that includes: board membership.

Data Availability

Data will be made available on request.

Acknowledgments

All authors would like to acknowledge the Paul Scherrer Institute, Villigen, Switzerland for provision of synchrotron radiation beamtime at the beamline cSAXS of the SLS and Christian Appel and Marianne Liebi for support during the experiments. Part of this work was carried out at the Chalmers Materials Analysis Laboratory, CMAL. MA and AS would like to thank the Knut and Alice Wallenberg foundation through their Wallenberg Academy Fellow program and the Area of Advance for Materials Science at Chalmers University of Technology for funding. AKR is employed at Amferia AB.

Appendix A. Supporting information

Supplementary data associated with this article can be found in the online version at doi:10.1016/j.colsurfb.2023.113304.

References

[1] R. Yoda, Elastomers for biomedical applications, J. Biomater. Sci. Polym. Ed. 9 (1998) 561–626. https://doi.org/10.1163/156856298X00046.
[2] M. Zare, E.R. Ghomi, P.D. Venkatraman, S. Ramakrishna, Silicone-based biomaterials for biomedical applications: Antimicrobial strategies and 3D printing technologies, J. Appl. Polym. Sci. 138 (2021) 50969, https://doi.org/10.1002/app.50969.
[3] Q. Chen, S. Liang, G.A. Thouas, Elastomeric biomaterials for tissue engineering, Prog. Polym. Sci. 38 (2013) 584–671, https://doi.org/10.1016/j.progpolymsci.2012.05.003.
[4] S.M. Jacobsen, D.J. Stickler, H.L.T. Mobley, M.E. Shirtliff, Complicated catheter-associated urinary tract infections due to escherichia coli and proteus mirabilis, Clin. Microbiol. Rev. 21 (2008) 26–59, https://doi.org/10.1128/CMR.00019-07.
[5] S. Li, S. Dong, W. Xu, S. Tu, L. Yan, C. Zhao, J. Ding, X. Chen, Antibacterial Hydrogels, Adv. Sci. 5 (2018) 1700527, https://doi.org/10.1002/advs.201700527.
[6] I. Pereira, C. Rodrigues, A. Rodrigues, M. Oliveira, M. Gama, Injectable hydrogels as a delivery system for bone regeneration, in: Bioinspired Mater. Med. Appl., Elsevier, 2017: pp. 241–271. https://doi.org/10.1016/B978-0-08-100741-9.00009-7.
[7] M. Saidi, A. Dabbaghi, S. Rahmani, Swelling and drug delivery kinetics of click-synthesized hydrogels based on various combinations of PEG and star-shaped PCL: influence of network parameters on swelling and release behavior, Polym. Bull. 77 (2020) 3989–4010, https://doi.org/10.1007/s00289-019-02948-z.
[8] A. Sivashanmugam, R. Arun Kumar, M. Vishnu Priya, S.V. Nair, R. Jayakumar, An overview of injectable polymeric hydrogels for tissue engineering, Eur. Polym. J. 72 (2015) 543–565, https://doi.org/10.1016/j.eurpolymj.2015.05.014.
[9] A.M.S. Costa, J.F. Mano, Extremely strong and tough hydrogels as prospective candidates for tissue repair – a review, Eur. Polym. J. 72 (2015) 344–364, https://doi.org/10.1016/j.eurpolymj.2015.07.053.
[10] J.Y. Sun, X. Zhao, W.R.K. Illeperuma, O. Chaudhuri, K.H. Oh, D.J. Mooney, J. J. Vlassak, Z. Suo, Highly stretchable and tough hydrogels, Nature 489 (2012) 133–136, https://doi.org/10.1038/nature11409.
[11] H. Yuk, T. Zhang, G.A. Parada, X. Liu, X. Zhao, Skin-inspired hydrogel-elastomer hybrids with robust interfaces and functional microstructures, Nat. Commun. 7 (2016) 1–11, https://doi.org/10.1038/ncomms12028.
[12] J. Cui, M.A. Lackey, G.N. Tew, A.J. Crosby, Mechanical properties of end-linked PEG/PDMS hydrogels, Macromolecules 45 (2012) 6104–6110, https://doi.org/10.1021/ma300593g.
[13] Y. Qin, Applications of advanced technologies in the development of functional medical textile materials, in: Med. Text. Mater., Elsevier, 2016: pp. 55–70. https://doi.org/10.1016/B978-0-08-100618-4.00005-4.
[14] A. Abdilla, C.A. D'Ambra, Z. Geng, J.J. Shin, M. Czuczola, D.J. Goldfeld, S. Biswas, J.M. Mecca, S. Swier, T.D. Bekemeier, D.S. Laitar, M.W. Bates, C.M. Bates, C. J. Hawker, Silicone-based polymer blends: enhancing properties through compatibilization, J. Polym. Sci. 59 (2021) 2114–2128, https://doi.org/10.1002/pol.20210453.
[15] P. Lucas, J.-J. Robin, Silicone-Based Polymer Blends: An Overview of the Materials and Processes, in: Funct. Mater. Biomater., Springer Berlin Heidelberg, Berlin, Heidelberg, 2007: pp. 111–147. https://doi.org/10.1007/12_2007_115.
[16] F. Abbasi, H. Mirzadeh, A.A. Katbab, Modification of polysiloxane polymers for biomedical applications: a review, Polym. Int. 50 (2001) 1279–1287, https://doi.org/10.1002/pi.783.
[17] M. Tsoka, P. Oikonomou, K.G. Papadokostaki, M. Sanopoulou, Properties of polydimethylsiloxane modified by blending with polyvinylpyrrolidone and a poly (ethylene oxide)-poly(propylene oxide) triblock copolymer, Ind. Eng. Chem. Res. 59 (2020) 5797–5807, https://doi.org/10.1021/acs.iecr.9b06691.
[18] U. Jorzik, B.A. Wolf, Reduction of the interfacial tension between poly (dimethylsiloxane) and poly(ethylene oxide) by block copolymers: effects of molecular architecture and chemical composition, Macromolecules 30 (1997) 4713–4718, https://doi.org/10.1021/ma9613300.

[19] S. Abdurrahmanoglu, V. Can, O. Okay, Design of high-toughness polyacrylamide hydrogels by hydrophobic modification, Polymer 50 (2009) 5449–5455, https://doi.org/10.1016/j.polymer.2009.09.042.
[20] M. Prévôt, S. Ustunel, E. Hegmann, Liquid crystal elastomers—a path to biocompatible and biodegradable 3D-LCE scaffolds for tissue regeneration, Materials 11 (2018) 377, https://doi.org/10.3390/ma11030377.
[21] E.-K. Fleischmann, R. Zentel, Liquid-crystalline ordering as a concept in materials science: from semiconductors to stimuli-responsive devices, Angew. Chem. Int. Ed. 52 (2013) 8810–8827, https://doi.org/10.1002/anie.201300371.
[22] M. Hussain, E.I.L. Jull, R.J. Mandle, T. Raistrick, P.J. Hine, H.F. Gleeson, Liquid crystal elastomers for biological applications, Nanomaterials 11 (2021) 813, https://doi.org/10.3390/nano11030813.
[23] S.W. Ula, N.A. Traugutt, R.H. Volpe, R.R. Patel, K. Yu, C.M. Yakacki, Liquid crystal elastomers: an introduction and review of emerging technologies, Liq. Cryst. Rev. 6 (2018) 78–107, https://doi.org/10.1080/21680396.2018.1530155.
[24] M.H. Li, P. Keller, M. Antonietti, D. Lacey, R.B. Meyer, Artificial muscles based on liquid crystal elastomers, Philos. Trans. R. Soc. A Math. Phys. Eng. Sci. 364 (2006) 2763–2777, https://doi.org/10.1098/rsta.2006.1853.
[25] J.D.W. Madden, N.A. Vandesteeg, P.A. Anquetil, P.G.A. Madden, A. Takshi, R. Z. Pytel, S.R. Lafontaine, P.A. Wieringa, I.W. Hunter, Artificial muscle technology: Physical principles and naval prospects, IEEE J. Ocean. Eng. 29 (2004) 706–728, https://doi.org/10.1109/JOE.2004.833135.
[26] S. Petsch, R. Rix, B. Khatri, S. Schuhladen, P. Müller, R. Zentel, H. Zappe, Smart artificial muscle actuators: Liquid crystal elastomers with integrated temperature feedback, Sens. Actuators, A Phys. 231 (2015) 44–51, https://doi.org/10.1016/j.sna.2014.10.014.
[27] M.E. Prévôt, H. Andro, S.L.M. Alexander, S. Ustunel, C. Zhu, Z. Nikolov, S. T. Rafferty, M.T. Brannum, B. Kinsel, L.T.J. Korley, E.J. Freeman, J.A. McDonough, R.J. Clements, E. Hegmann, Liquid crystal elastomer foams with elastic properties specifically engineered as biodegradable brain tissue scaffolds, Soft Matter 14 (2018) 354–360, https://doi.org/10.1039/C7SM01949A.
[28] A. Sharma, A. Neshat, C.J. Mahnen, A.D. Nielsen, J. Snyder, T.L. Stankovich, B. G. Daum, E.M. Laspina, G. Beltrano, Y. Gao, S. Li, B.W. Park, R.J. Clements, E. J. Freeman, C. Malcuit, J.A. McDonough, L.T.J. Korley, T. Hegmann, E. Hegmann, Biocompatible, biodegradable and porous liquid crystal elastomer scaffolds for spatial cell cultures, Macromol. Biosci. 15 (2015) 200–214, https://doi.org/10.1002/mabi.201400325.
[29] T.J. White, D.J. Broer, Programmable and adaptive mechanics with liquid crystal polymer networks and elastomers, Nat. Mater. 14 (2015) 1087–1098, https://doi.org/10.1038/nmat4433.
[30] R.S. Kularatne, H. Kim, J.M. Boothby, T.H. Ware, Liquid crystal elastomer actuators: synthesis, alignment, and applications, J. Polym. Sci. Part B Polym. Phys. 55 (2017) 395–411, https://doi.org/10.1002/polb.24287.
[31] C.P. Ambulo, J.J. Burroughs, J.M. Boothby, H. Kim, M.R. Shankar, T.H. Ware, Four-dimensional printing of liquid crystal elastomers, ACS Appl. Mater. Interfaces 9 (2017) 37332–37339, https://doi.org/10.1021/acsami.7b11851.
[32] A.V. Abadia, K.M. Herbert, T.J. White, D.K. Schwartz, J.L. Kaar, Biocatalytic 3D actuation in liquid crystal elastomers via enzyme patterning, ACS Appl. Mater. Interfaces 14 (2022) 26480–26488, https://doi.org/10.1021/acsami.2c05802.
[33] Y. Jiang, X. Dong, S. Zhu, S. Dai, H. Bai, Q. Li, L. Li, N. Yuan, J. Ding, Skin-friendly and antibacterial monodomain liquid crystal elastomer actuator, Colloids Surf. B Biointerfaces 222 (2023), 113110, https://doi.org/10.1016/j.colsurfb.2022.113110.
[34] W. Li, M. Khan, L. Lin, Q. Zhang, S. Feng, Z. Wu, J.M. Lin, Monitoring H2O2 on the surface of single cells with liquid crystal elastomer microspheres, Angew. Chem. - Int. Ed. 59 (2020) 9282–9287, https://doi.org/10.1002/anie.202004326.
[35] H. Zeng, O.M. Wani, P. Wasylczyk, R. Kaczmarek, A. Priimagi, Self-regulating iris based on light-actuated liquid crystal elastomer, Adv. Mater. 29 (2017) 1701814, https://doi.org/10.1002/adma.201701814.
[36] R.K. Shaha, D.R. Merkel, M.P. Anderson, E.J. Devereaux, R.R. Patel, A.H. Torbati, N. Willett, C.M. Yakacki, C.P. Frick, Biocompatible liquid-crystal elastomers mimic the intervertebral disc, J. Mech. Behav. Biomed. Mater. 107 (2020), 103757, https://doi.org/10.1016/j.jmbbm.2020.103757.
[37] M.O. Saed, R.H. Volpe, N.A. Traugutt, R. Visvanathan, N.A. Clark, C.M. Yakacki, High strain actuation liquid crystal elastomers via modulation of mesophase structure, Soft Matter 13 (2017) 7537–7547, https://doi.org/10.1039/c7sm01380a.
[38] J. Maeng, R.T. Rihani, M. Javed, J.S. Rajput, H. Kim, I.G. Bouton, T.A. Criss, J. J. Pancrazio, B.J. Black, T.H. Ware, Liquid crystal elastomers as substrates for 3D, robust, implantable electronics, J. Mater. Chem. B 8 (2020) 6286–6295, https://doi.org/10.1039/d0tb00471e.
[39] T. Turiv, J. Krieger, G. Babakhanova, H. Yu, S.V. Shiyanovskii, Q.-H. Wei, M.-H. Kim, O.D. Lavrentovich, Topology control of human fibroblast cells monolayer by liquid crystal elastomer, Sci. Adv. 6 (2020), https://doi.org/10.1126/sciadv.aaz6485.
[40] A. Agrawal, O. Adetiba, H. Kim, H. Chen, J.G. Jacot, R. Verduzco, Stimuli-responsive liquid crystal elastomers for dynamic cell culture, J. Mater. Res. 30 (2015) 453–462, https://doi.org/10.1557/jmr.2014.392.
[41] A. Stepulane, A.K. Rajasekharan, M. Andersson, Multifunctional surface modification of PDMS for antibacterial contact killing and drug-delivery of polar, nonpolar, and amphiphilic drugs, ACS Appl. Bio Mater. 2022 (2022) 5289–5301, https://doi.org/10.1021/acsabm.2c00705.
[42] S. Atefyekta, E. Blomstrand, A.K. Rajasekharan, S. Svensson, M. Trobos, J. Hong, T. J. Webster, P. Thomsen, M. Andersson, Antimicrobial peptide-functionalized mesoporous hydrogels, ACS Biomater. Sci. Eng. 7 (2021) 1693–1702, https://doi.org/10.1021/acsbiomaterials.1c00029.
[43] E. Blomstrand, A.K. Rajasekharan, S. Atefyekta, M. Andersson, Cross-linked lyotropic liquid crystal particles functionalized with antimicrobial peptides, Int. J. Pharm. 627 (2022), 122215, https://doi.org/10.1016/j.ijpharm.2022.122215.
[44] K.W. Chun, J.B. Lee, S.H. Kim, T.G. Park, Controlled release of plasmid DNA from photo-cross-linked pluronic hydrogels, Biomaterials 26 (2005) 3319–3326, https://doi.org/10.1016/j.biomaterials.2004.07.055.
[45] P. Holmqvist, P. Alexandridis, B. Lindman, Modification of the microstructure in block copolymer−water−“oil” systems by varying the copolymer composition and the “oil” type: small-angle X-ray scattering and deuterium-NMR investigation, J. Phys. Chem. B 102 (1998) 1149–1158, https://doi.org/10.1021/jp9730297.
[46] A.K. Rajasekharan, C. Gyllensten, E. Blomstrand, M. Liebi, M. Andersson, Tough ordered mesoporous elastomeric biomaterials formed at ambient conditions, ACS Nano (2019), https://doi.org/10.1021/acsnano.9b01924.
[47] W.-X. He, A.K. Rajasekharan, A.R. Tehrani-Bagha, M. Andersson, Mesoscopically ordered bone-mimetic nanocomposites, Adv. Mater. 27 (2015) 2260–2264, https://doi.org/10.1002/adma.201404926.
[48] P. Kraft, A. Bergamaschi, C. Broennimann, R. Dinapoli, E.F. Eikenberry, B. Henrich, I. Johnson, A. Mozzanica, C.M. Schlepütz, P.R. Willmott, B. Schmitt, Performance of single-photon-counting PILATUS detector modules, J. Synchrotron Radiat. 16 (2009) 368, https://doi.org/10.1107/S0909049509009911.
[49] B. Henrich, A. Bergamaschi, C. Broennimann, R. Dinapoli, E.F. Eikenberry, I. Johnson, M. Kobas, P. Kraft, A. Mozzanica, B. Schmitt, PILATUS: A single photon counting pixel detector for X-ray applications, Nucl. Instruments Methods Phys. Res. Sect. A Accel. Spectrometers, Detect. Assoc. Equip. 607 (2009) 247–249. https://doi.org/10.1016/J.NIMA.2009.03.200.
[50] P. Holmqvist, P. Alexandridis, B. Lindman, Phase behavior and structure of ternary amphiphilic block copolymer−alkanol−water systems: comparison of poly (ethylene oxide)/poly(propylene oxide) to poly(ethylene oxide)/poly (tetrahydrofuran) copolymers, Langmuir 13 (1997) 2471–2479, https://doi.org/10.1021/la960819j.
[51] P. Holmqvist, P. Alexandridis, B. Lindman, Modification of the microstructure in poloxamer Block copolymer-water-"oil" systems by varying the “oil” type, Macromolecules 30 (1997) 6788–6797, https://doi.org/10.1021/ma970625q.
[52] B. Svensson, P. Alexandridis, U. Olsson, Self-assembly of a poly(ethylene oxide)/poly(propylene oxide) block copolymer (pluronic P104, (EO)27(PO)61(EO)27) in the presence of water and xylene, J. Phys. Chem. B 102 (1998) 7541–7548, https://doi.org/10.1021/jp981789r.
[53] A. Rodriguez-Palomo, V. Lutz-Bueno, M. Guizar-Sicairos, R. Kádár, M. Andersson, M. Liebi, Nanostructure and anisotropy of 3D printed lyotropic liquid crystals studied by scattering and birefringence imaging, Addit. Manuf. 47 (2021), 102289, https://doi.org/10.1016/j.addma.2021.102289.
[54] V. Guarino, F. Causa, L. Ambrosio, Porosity and mechanical properties relationship in PCL porous scaffolds, 149–57, J. Appl. Biomater. Biomech. 5 (2007), https://doi.org/10.1177/228080000700500303.
[55] S.-H. Park, H.-K. Choi, The effects of surfactants on the dissolution profiles of poorly water-soluble acidic drugs, Int. J. Pharm. 321 (2006) 35–41, https://doi.org/10.1016/j.ijpharm.2006.05.004.
[56] M.L. Veyries, G. Couarraze, S. Geiger, F. Agnely, L. Massias, B. Kunzli, F. Faurisson, B. Rouveix, Controlled release of vancomycin from Poloxamer 407 gels, Int. J. Pharm. 192 (1999) 183–193, https://doi.org/10.1016/S0378-5173(99)00307-5.
[57] A.K. Rajasekharan, R. Bordes, C. Sandström, M. Ekh, M. Andersson, Hierarchical and heterogeneous bioinspired composites—merging molecular self-assembly with additive manufacturing, Small 13 (2017) 1–11, https://doi.org/10.1002/smll.201700550.